SwissCube: development of an ultra-light and efficient Inertia Wheel for the attitude control and stabilization of CubeSat class satellites

Author:
Gavrilo Bozovic, Swiss Federal Institute for Technology (EPFL), Laboratory of Integrated Actuators (LAI), Switzerland
gavrilo.bozovic@gmail.com

Co-authors:
Omar Scaglione, EPFL-LAI, Switzerland, omar.scaglione@epfl.ch
Christian Koechli, EPFL-LAI, Switzerland, christian.koechli@epfl.ch
Muriel Noca, EPFL Space Center, Switzerland, muriel.noca@epfl.ch
Yves Perriard, EPFL-LAI, Switzerland, yves.perriard@epfl.ch

1 INTRODUCTION

An increasing number of CubeSats are being developed around the world. However, for the moment, there is no means of controlling accurately the attitude of these satellites, without affecting significantly the space, weight and power available for the payload in the satellite.

The aim of this project was to develop an Inertia Wheel Assembly (IWA), which could be integrated in a CubeSat, with a shape allowing it not to interfere with the satellite's other components, as well as a minimal weight and energy consumption.

The scientific mission of the SwissCube is to make measurements of the NightGlow, a luminescence phenomenon of the atomic oxygen, at high levels of the atmosphere. For this, the SwissCube will take images of these layers of the atmosphere, using a custom camera placed along its X axis.

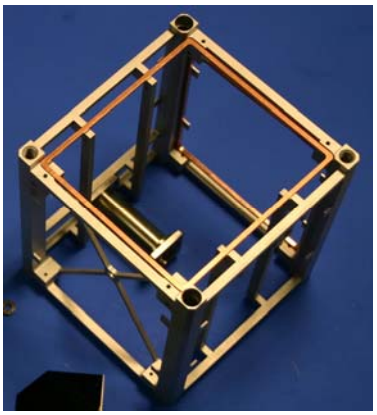

Figure 1 . Aluminium structure of the SwissCube. Note the cylinder, which is the frame for the objective of the payload's CCD camera, and the X frame, where the IWA is to be mounted. In addition, dummy magnetotorquers are visible, in copper color.

The intent of the SwissCube mission was to demonstrate the function of the IWA, with one wheel placed on the Y axis. This disposition is visible in Figure 1. This way, the IWA can be used to stabilize the camera by applying a constant speed, which generates a gyroscopic effect. In addition, accelerating or slowing the wheel allows compensating for perturbations, and allows orienting the

satellite, so that it always points to the horizon.

The purpose of this paper is to present the application of modern optimization techniques to the design of the flywheel drive.

2 SPECIFICATIONS

The key specifications for the system are described in this section. The duration of the mission is 1 year.

2.1 Temperature

The motor shall operate under vacuum conditions at a temperature range between -20° [C] and 80° [C].

2.2 Dimensions

The room for the wheel is very limited: In order not to interfere with the payload, the wheel is located in the side of the satellite. Its diameter shall not exceed 80 [mm] and its thickness shall not be bigger than 8 [mm]. This allows an easy assembly, while being in locations usually not occupied by the payload. The total weight of the system shall be less than 37.5[g], for one IWA (13.5 [g] for the wheel, 7 [g] for the support, 15 [g] for the motor and 2 [g] for the electronics).

2.3 Power

The mean available power is 100 [mW], with a 3.3 [V] voltage.

2.4 Inertia, torque and speed

The Attitude Determination and Control Systems (ADCS) team has determined the following parameters to guarantee that the satellite remains stable: The inertia of the rotating part shall be of 2.16 10-5 [kg m2] within 1%. The wheel will be rotating between 5000 and 11000 [rpm] with a 10 [rpm] tolerance, making it important for the control algorithm to measure and control the speed with precision. The lower boundary of 5000 [rpm] is defined so that the IWA can provide a sufficient inertial moment for the stiffening of the axis of the satellite.

The IWA shall be able to provide a torque sufficient to compensate for the worst-case perturbations that the satellite will face. This torque $T_{\min}$ is defined as:

$$T_{\min} = 6T_{fr} + 2.5T_{dyn} \quad (1)$$

Where T_{fr} is the friction torque and T_{dyn} is the dynamical torque, which is the worst case for the torque generated by the perturbations. The obtained value for $T_{\min}$ is 37.5 [μNm]. This torque, with the inertia presented above, leads to an acceleration of 3000 [rpm] during one revolution of the Earth, which is 90 minutes. The upper limit of the speed, at 11 000 [rpm], was set so that the satellite can compensate for the worst-case perturbations during two full revolutions. If the upper limit speed is reached, the drive has to be slowed down, stabilizing the satellite using the magetotorquers.

2.5 Additional constraints

While designing a device for a spatial application, one has to consider the high mechanical stress that the device will have to endure during the launch. The worst-case conditions considered for this design are the ones of the DNEPR launcher. The drive therefore has to resist to 10.4 [g] accelerations, and it shouldn't have any eigenfrequency in the 30-100 [Hz] range, which is the vibration range of the launchers

In addition, in order not to interfere with the attitude determination, done with magnetometers, among others, the magnetic flux leakage of the drive has to be limited to less than 1% of the worst case earth induction. Therefore, the induction of the drive at the location of the magnetometer should be inferior to $1.94 \cdot 10^{-7}$ [T].

3 MOTOR DESIGN

The methodology used to design the motor is as follows:

1. Down selection of the motor type according to the mission specifications
2. Selection of the most suitable geometry, for the selected motor type
3. Selection of the number of coils and poles
4. Creation of an analytical model of the selected geometry
5. Non-linear, multi-parameter optimization of the analytical model, using an optimization software
6. Verification of the results of the model using FEA and fine-tuning of the parameters
7. Construction of a prototype and validation of the model

3.1 Type of motor

The first choice to be done is the motor type. The possible choices from least to most interesting motor type are listed below:

A) **The DC (brushed) motor** is believed to be less reliable at higher speed than its brushless variant. In addition, the slip ring requires space, introduces friction and can generate debris, which may reach a sensitive part of the satellite and damage it.

B) **The hybrid stepper motor** is not an efficient solution at high speeds.

C) **The Induction motor** is less efficient than the brushless variant; it has low iron losses at higher speed under no load. Another point against its use is that there are very few applications, if any, of this type of motor in the 100mW range.

D) **PM Synchronous "brushless" motor**. This motor type was considered as the most suitable for our application, due to its high efficiency, even at high speeds, mainly.

3.2 Geometry selection

Three geometries were considered for this drive:

- **Internal rotor motor** are less interesting, as, for a given space and mass, they have less inertia than the following geometry
- **Motors with external rotor** (see Figure 2) have been used for applications in the same range of power. However, in a motor whose diameter is larger than its length, the end turns of the coils of a radial flux drive generate an important loss of space.

- **Axial flux motors** (see Figure 3) allow having a very flat design. In addition, the end turns unwind radially, where space is less restrictive in our case. [4][5]

Figure 2 . PM synchronous "Brushless" motor with external rotor

All these variants can be either slotted or slotless. The slotless variant has been selected for two reasons:

- A slotted drive has a preferred position, with the magnets facing the teeth of the stator yoke. This generates high torque oscillations if the drive is stopped, which would affect the satellite attitude. In addition, this preference implies that a higher torque has to be applied on the drive to start it.
- In the slotless design, as can be seen in Fig. 3, the coils are placed between the rotor yoke, which is the one bearing the magnets, and the stator yoke. This is done at the expense of a new air gap, but prevents torque oscillations. In addition, this geometry does not require a static stator yoke. In our design, a mechanical coupling (not visible in Figure 3) exists between the yoke that bears the magnets, and the one on the other side of the coils. This way, there are no Eddy-current losses due to the variation of the flux generated by the permanent magnets, in the stator yoke. These losses are a major concern in high-speed drives.

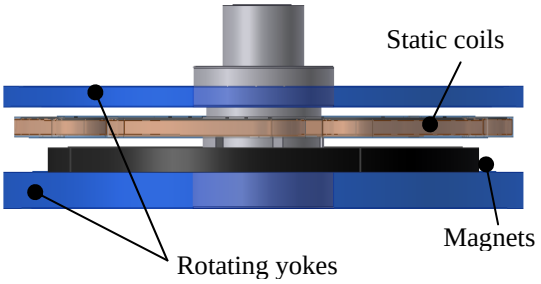

Figure 3 . Axial flux PM synchronous "Brushless" motor

For these reasons, the axial flux, permanent magnet, slotless, synchronous motor was chosen. However, a radial flux structure was also optimized, to provide a comparison point.

Note that the impact of the Eddy currents on the performances of motors is usually limited by using stacked sheet metal yokes. In this situation, the metal sheets have to be parallel to the magnetic flux, as the Eddy current appear in perpendicular planes. While this is a good solution for radial flux structures, it cannot be applied for axial flux drives, as the flux travels in the yokes on arc shaped paths. The metal sheets should therefore be thin concentric crowns, or a spiral, which are not available production methods.

3.3 Number of coils and pole pairs selection

The number of phases has been chosen equal to three to simplify the sensorless control of the motor. The concentric winding is the easiest to manufacture, if not the only possible choice in this case.

The number of phases implies that the number of coils must be a multiple of 3. Due to the size restrictions, it would be very difficult to mount more than three or six coils. The possible pole / coils combinations are the following: 3 coils / 2 poles, 3 coils / 4 poles, 6 coils / 4 poles, 6 coils / 8 poles. The bipolar motor has quickly been eliminated because its yokes would be too thick.

The three last configurations were introduced into the optimization model, for the final selection.

3.4 Design optimization

The optimization of the motor has been done in two steps:

- Pre-design using non-linear programming [8] with the Pro@Design software, which requires an analytical model of the system.
- FEA simulations for:
  - Tuning the parameters
  - Checking the level of the magnetic flux leakage
  - Checking the structural behavior of the assembly

3.4.1 Analytical model

For the optimization to be efficient, a multiphysical analytical model of the drive was built, integrating the electromechanical forces, as well as the geometry and the final inertia of the whole IWA.

In Figure 4 is presented a cut through the drive, presenting the different components, and their dimensional parameters.

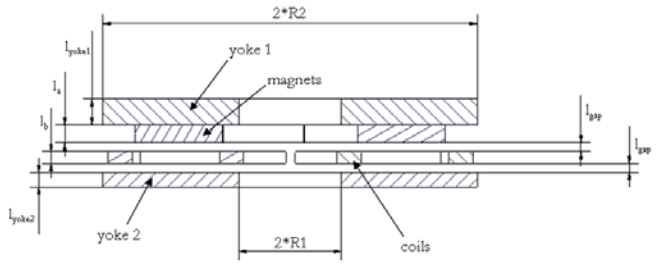

Figure 4 : cut through the motor, with dimensional paramters

As the most problematic resource in the satellite is energy, the goal of the optimization was to obtain a drive with maximal efficiency, using the maximal space and weight allowed.

3.4.1.1 Assumptions

Following assumptions were made for the analytical model:

- There are no losses of magnetic flux. After the optimization of the drive is finished under this

assumption, the losses have to be calculated using FEA simulations, or determined measuring the back EMF in a prototype. Parameters (mainly the number of turns in the coils) can then be fine-tuned.

- There are no Eddy current losses. As was commented before, the rotation of both yokes suppresses the variation of flux that are caused by the motion of the permanent magnets. Small losses may still exist, due to the magnetic flux generated by the coils. However, the intensity of these magnetic flux is several orders of magnitude inferior to the ones generated by the magnets.

3.4.1.2 Additional constraints

Further boundaries had to be applied to the model, due to:

- Dimensions of standard components to be added in the drive, mainly the ball bearings. For this application, Myonic bearings were used, for their small size, and availability with solid lubrication.
- Manufacturing capabilities
- Resistance to the mechanical loads, mainly during the launch

3.4.1.3 Wheel design

In Figure 5 is schematically represented the inertia wheel itself, from a top view. The parameters labeled in this figure were implemented in the analytical model, which calculated the inertia as well. As it is visible, the drive is to be mounted in the center of the wheel, while the inertia itself is concentrated on the outer diameter, taking as much space is allowed, in order to minimize the weight for a given inertia. The center is linked to the outer ring by three arms. This number was selected due to following constraints:

- The arms bring mass in the center of the assembly, that does not contribute efficiently to the inertia. A minimal number of arms is therefore desired
- A 2-arm configuration would generate oscillations if the satellite was rotated around an axis perpendicular to the one of the IWA, while this device is in function

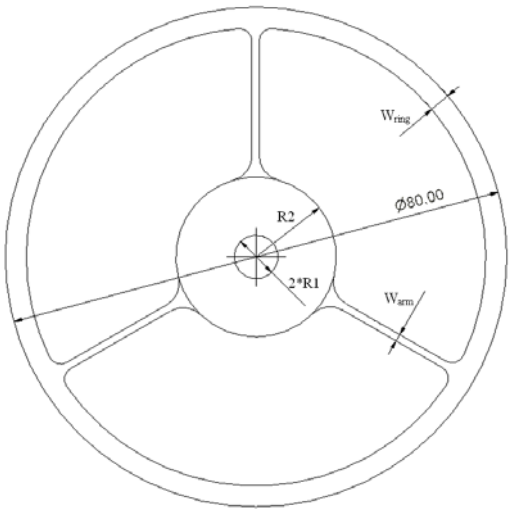

Figure 5 : Representation of the wheel itself, with its parameters

3.4.1.4 Materials

The chosen magnetic materials are soft iron (Armco) for the yokes and N40H NdFeB (B_0=1.3T) for the permanent magnets.

More efficient materials exist, for the yokes, such as the Iron-Boron alloys. However, these were not available for this project. The limiting criterion for the selection of the magnet material is the resistance to the temperature. Indeed, some NdFeB materials have curie points under 80° [C], which would have led to the demagnetization of the magnets, on the long run.

The wheel itself was built out of 7022 Certal Aluminum, chosen for its high Young modulus, easy machining, and low density.

3.4.1.5 Optimization results

Table 1 contains the results for the different optimized coil / pole configurations, as well as for the external rotor geometry. It is noteworthy that the radial flux geometry presents significantly lower performances. This can be attributed to the end turns of the coils that unwind axially, thus limiting the useful length of the drive.

TABLE I
OPTIMIZATION RESULTS

Motor Type	Coil Count	Pole Count	Motor Efficiency [%]
Axial Flux	3	4	96.6
Axial Flux	6	4	97.8
Axial Flux	6	8	97.8
External Rotor			74.3

The 3 coil configuration has lower performances. In addition, 120° coils of such small sizes present production and handling issues. Therefore, the 6 coils configuration was selected.

According to the optimization model, both the 4 and the 8 poles configurations should have the same performances. However, the 8 pole motor is bound to have induced voltages closer to a sine curve, and therefore with less harmonics. Harmonics represent power losses to torque oscillations. Therefore, a 6 coils, 8 poles drive was built.

The calculations indicate that the Joule effect losses are very low, inferior to 1 [mW]. Therefore, no thermal simulation of the drive was required, as it was assumed that the satellite frame would dissipate the generated heat.

The drive and the wheel, according to the optimized dimensions, are presented in Figure 6. This figure presents the different parts as they were schematically presented for the design, and prior to an actual design

Figure 6 Motor and wheel assembly. This figure presents the drive with its actual dimensions, but prior to the actual mechanical design.

4 SIMULATIONS

4.1 Induction in the yokes and back EMF

The variants have been analysed and simulated using 3D FEA (Figure 7) and a lumped-model, which was developed in house (Figure 8) to allow for quicker analysis.

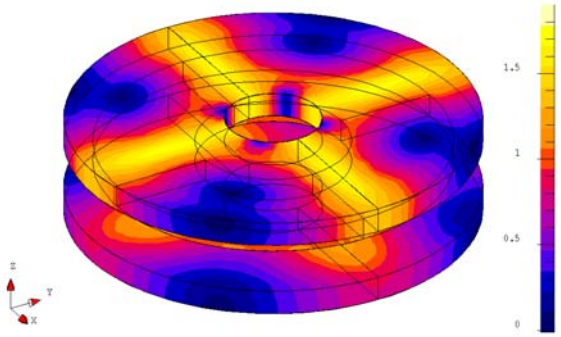

Figure 7 Flux density [T] in the yokes, for a 4 poles drive

The Flux density in the yokes has been represented in Figure 7 for the 4-pole motor. Figure 8 shows the harmonic filtering effect of the winding in comparing the back-EMF of the 3 phases of the 4-pole motor with its 8-pole counterparts.

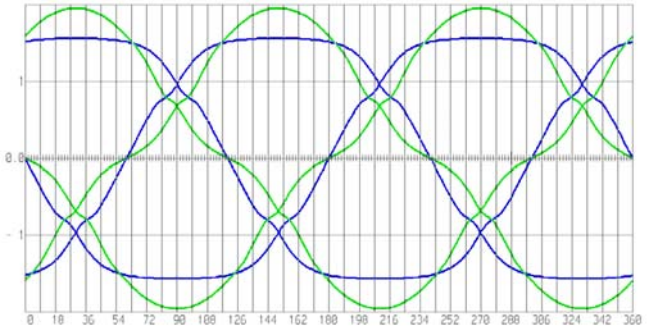

Figure 8 Phase Back-EMF voltages of the 3 phases[V] vs. electrical degrees (4-pole motor in green, 8-pole motor in blue)

4.2 Induction outside of the drive

In Figure 9 is presented the result of one of the simulations run to determine the induction generated by the drive, outside of the motor. The surface on which the magnetic induction is calculated represents one PCB in the satellite. It is visible that a local minimum of the induction is present in the axis of the drive. According to the results, presented in Figure 10, the drive should not have an impact on the magnetometer measurements, as long as the magnetometer is placed more than 30 [mm] away from the drive, and in its axis. In a case where a full 3 IWA system is used, the magnetometer should be in the center of the satellite.

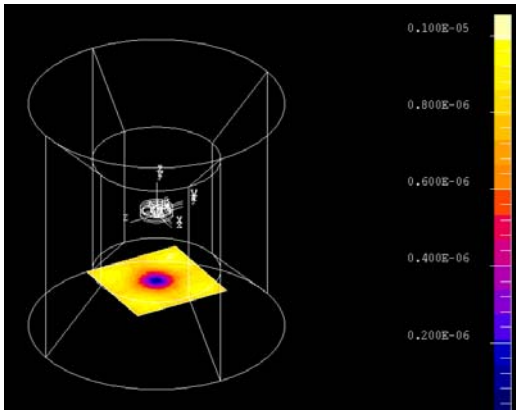

Figure 9 Simulation of the induction outside of the motor

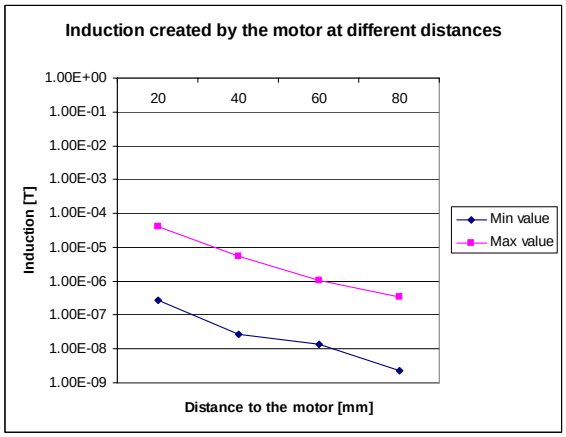

Figure 10 Maximal and minimal induction on planes at different distances of the drive

4.3 Mechanical aspect

Simulations were run on the wheel itself to determine its resistance to mechanical loads. The first mode of vibration is represented in Figure 11. The associated eigenfrequency is of 1490 [Hz]. This mode could be excited by the launcher's axial vibrations. However, the typical range of vibration frequencies for the launchers is 30-100 [Hz].

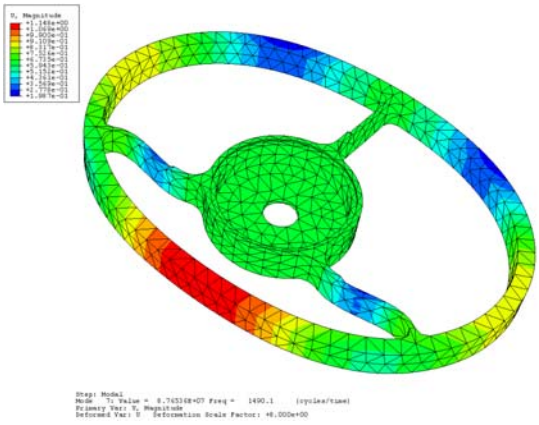

Figure 11 First mode of vibration

The second mode of vibration is presented in Figure 12. This vibration is rotational, and could be caused by the drive's harmonics torque oscillations. The highest torque oscillation frequency is at the drive's 7th harmonic, which is, for 11 000 [rpm], at 1 283 [Hz]. However, the eigenfrequency associated to this vibration mode is higher, at 2090 [Hz].
If a mechanical issue was spotted, the wheel should have been redesigned in a stiffer way, which would have lead to a higher mass.

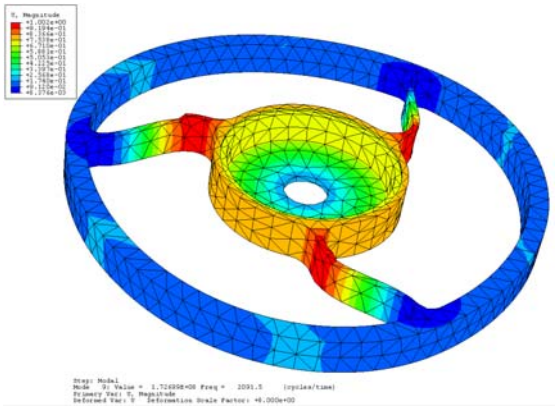

Figure 12 Second mode of vibration

5 MECHANICAL DESIGN

The only static element in the drive is a central swivel, and the coils, such as it is represented in Figure 13. The coils are molded in an epoxy disk, which holds them together and to the central swivel. The swivel itself is hollow, and has 6 slots, allowing to pass the cables from the coils to the electronics. This component can be seen in Figure 14.

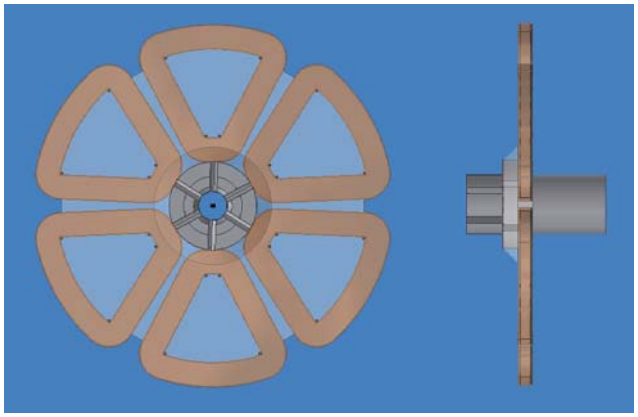

Figure 13 Projection of the static part of the drive. Diameter = 25 [mm]

Figure 14 Central swivel

The mold used for the casting of the epoxy is presented in Figure 15.

Figure 15 parts of the mould. Left : male part with surplus evacuations. Right : female part. Note the tops of the extraction screws confounded with the bottom of the mould.

The full assembly is then represented in Figure 16. As it is visible, one yoke is mounted in the bottom of the inertia wheel. Both parts are bonded using Epoxy resin, and a ball bearing is press-fitted in their inner radius. The central swivel with the coils can then be inserted in place. The second yoke, with the magnets, is inserted over the swivel, and is guided by a flange in the inertia wheel. In a drive for an actual space mission, this yoke would be bonded to the wheel with resin. However, this doesn't have to be done for the tests, as it holds by itself, due to the strong magnetic attraction of both yokes.
A cut through the drive is presented in Figure 17, and pictures of the drive at different stages of the assembly in Figure 18.

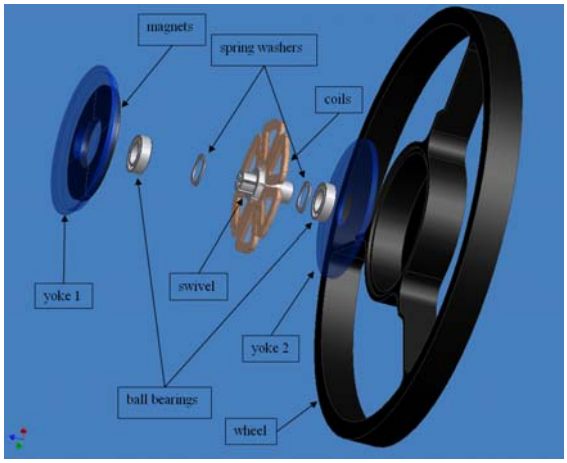

Figure 16 Drive assembly

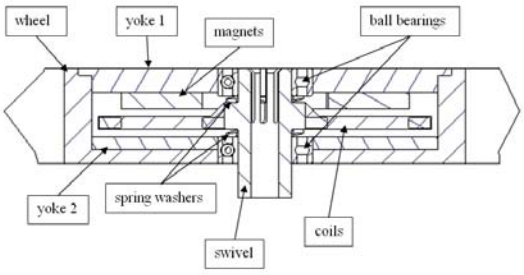

Figure 17 Cut through the motor assembly

Figure 18 Assembly of the drive

6 Electronic Drive and Control

A sensorless control electronic has been developed for the motor. All the test data presented in the next sections was obtained using this electronic driver.

The computing time available on the satellite is very limited, in order to leave as much computational time as possible to the payload. Therefore, the simplest sensorless commutation technique, block commutation has been chosen. The zero crossings of the back-EMF are detected using analog electronics and a low-pass filter. Using these signals a microcontroller (8bit, low consumption MSP430 from Texas Instruments) generates the PWM and the commutation signals to command the power bridge. The CPU time is shared with the Altitude Control and Detection System (ADCS), which sets the speed of the wheel and enables the system (see Figure 19).

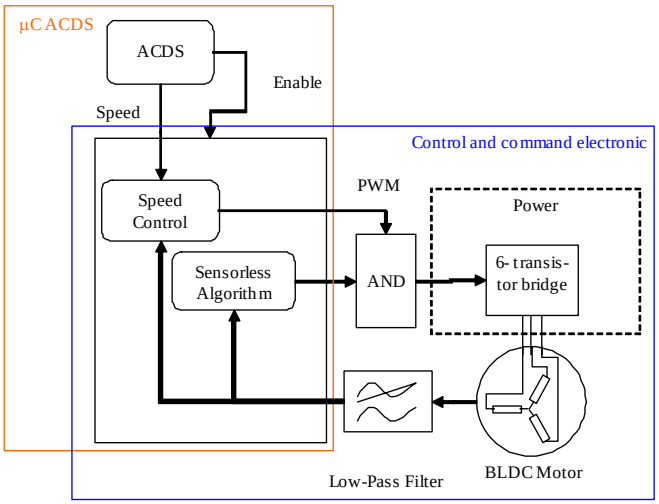

Figure 19 Functional representation of the control electronic

7 Tests

All the tests on the drive were run in a vacuum chamber, as otherwise, the friction of the air would have corrupted all the results. However, due to difficulties in shipment, standard ball bearings were used for these. This lead to an increased energy consumption, but allowed showing the functionality of the drive.

The back EMF in the drive, as well as its Fourier transform, are presented in Figure 20. It is visible that the intensity of the third harmonic is low, and that the back EMF is very close to a sine. This means that the torque oscillations are low, and that most of the consumed power generates torque, and not torque oscillations.

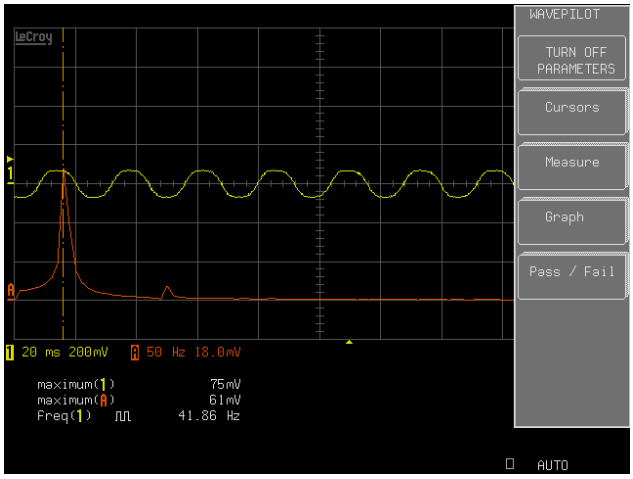

Figure 20 Back EMF and its Fourier transform (in orange). Note the very low intensity of the third harmonic

In Figure 21 is demonstrated the function of the back EMF zero detection. It is visible that a low-pass filter can efficiently remove the noise from the signal, without introducing a significant delay in the reading.

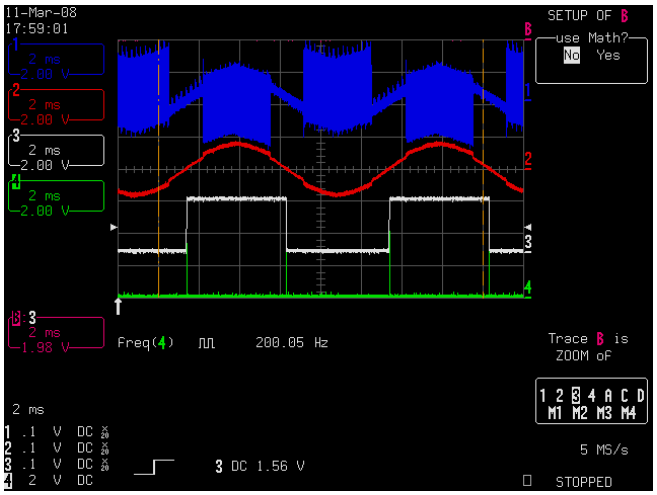

Figure 21 Blue: phase voltage. Red: filtered phase voltage. White: zero-detection signal. Green: commutation signal

The maximal speed reached with this drive was 15'500 [rpm], which is more than expected (11 000 [rpm]). The phase voltages, and the zero-detection curve, at this speed, are presented in Figure 22. The commutations in the phases are clearly visible in the phase voltage graphs. In the same figure is presented the RMS current consumption of the drive, which is 222.3 [mA]. With a 3.3 [V] supply voltage, this leads to an energy consumption of 735 [mW]. This is much more than what the drive was designed to. However, several elements can explain this discrepancy:

- The lack of lubrication of the ball bearings
- An insufficient vacuum level

Due to these, the energy performances of the drive will have to be further tested, in more adequate conditions. Nevertheless, the functionality of the drive was demonstrated, and, considering the high impact of the test material limitations, and the consistency of the other drive parameters with the simulations, we have good confidence that the final drive will reach its specifications.

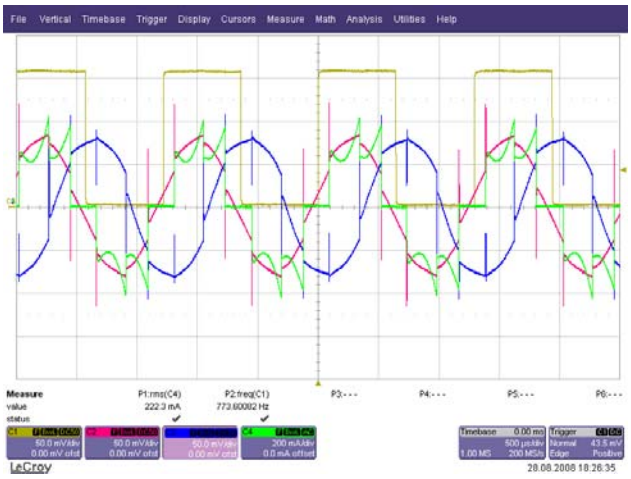

Figure 22 Phase voltages and zero-detection curve at the maximal speed

8 Conclusion

This publication presents the application of state-of-the art optimization and design techniques for the design of an inertia wheel assembly, suitable for the stabilization of pico-satellites.

The drive developed during this project has a particular structure, having two rotating yokes, and has a shape that allows its assembly in a CubeSat without consuming too much space, weight and energy, which are crucial for the payload. A drive was optimized, mechanically designed, and prototypes were built, as well as a low consumption, low CPU usage ad-hoc electronic driver. These allowed showing the good function of the drive, although further testing is required to reach full qualification.

The SwissCube, for which this wheel was built, will be launched by the fall of 2009. However, it but will not integrate this device, due to a conflict with other subsystems. Nevertheless, we showed that the developed system is functional, and could be applied to any CubeSat, provided its integration in the ADCS control software.

References

[1] "*Cubesat Design Specifications*" rev. 9. California Polytechnic State University San Luis Obispo / Stanford University, 2005.

[2] J. Puig-Suari, C. Turner, W. Ahlgren, "*Development of the standard CubeSat deployer and a CubeSat class PicoSatellite*", Aerospace Conference, 2001, IEEE Proceedings. Volume 1, 10-17 March 2001.

[3] Sang-Ho Lee, Su-Beom Park, Soon-O Kwon, Ji-Young Lee, Jung-Jong Lee, Jung-Pyo Hong, and Jin Hur "*Characteristic Analysis of the Slotless Axial-Flux Type Brushless DC Motors Using Image Method*", IEEE Transactions on Magnetics, vol. 42, N° 4, April 2006.

[4] R.Hanitsch, R. Belmans, R.Stephan, "*Small Axial Flux Motor with Permanent Magnet Excitation and Etched Airgap Winding*", IEEE Transactions on Magnetics, vol. 30, N° 2, March 1994.

[5] A. Cavagnino, M. Lazzari, F. Profumo and A. Tenconi, "*A Comparison between the Axial Flux and the Radial Flux Structures for PM Synchronous Motors*", IEEE Transactions on Industry Applications vol. 38, N°6, November/December 2002.

[6] N. Boules "Prediction of no-load flux density distribution in permanent magnet machines*" IEEE. Trans. Ind. Appl.*, vol. IA-21, pp. 633-643, May/June. 1985.

[7] B. Hague, *The principles of Electromagnetism Applied to Electrical Machines*, New York: Dover, 1962.

[8] C.Koechli, B. Fussell, S. Prina, D. James, Y. Perriard "*Design optimization of induction Motors for aerospace applications*", Proceeding Industry Applications Conference. Seattle, WA, 2004, vol. 4, pp 2501-2505.